Proceedings of ICRC 2001: 2721 © Copernicus Gesellschaft 2001

ICRC 2001

The influence of dust on the inverse Compton emission from jets in AGNi

C. Arbeiter, M. Pohl, and R. Schlickeiser

Institut für Theoretische Physik, Lehrstuhl IV: Weltraum- und Astrophysik, Ruhr-Universität Bochum, D-44780 Bochum, Germany

Abstract. The recently observed high energy γ-ray emission from more than sixty blazars is most likely caused by inverse Compton scattering of soft ambient photons, the source of which is a subject of extensive debate. We investigate the influence of a dust torus on the inverse Compton emission of the relativistic electrons in the jets of Active Galactic Nuclei. This is an extension of previous studies, in which the main focus had been on target photons emitted by the accretion disk. We show that due to the different angular distribution of the two photon fields, the beaming pattern of the respective scattered inverse Compton gamma rays are different. We also calculate the bolometric luminosity, the beaming pattern and the spectral distribution of the emitted gamma rays for the dust torus as well as for the accretion disk as the target photon source. The results show that the relative contributions of both to the gamma ray emission depend sensitively on the observer's viewing angle and the distance of the jet plasmoids from the accretion disk and the dust torus, respectively.

1 Introduction

The inverse Compton process has been considered a likely mechanism to produce the high energy γ-radiation from AGNi. In this process low energy photons are scattered by relativistic electrons and positrons within the jets. The low energy photons may penetrate the jet from outside *(Extern-Inverse-Compton scattering, EIC)* (Dermer et al., 1992) or they can be generated by the jet itself via synchrotron radiation *(Synchrotron-Self-Compton scattering, SSC)* (Maraschi et al., 1992). In the following the EIC scattering will be examined. We will, in particular emphasise the importance of the dust torus as a source of target photons and compare its contribution to the γ-ray production with the contribution of the scattered accretion disk photons.

Correspondence to: C. Arbeiter
(ca@tp4.ruhr-uni-bochum.de)

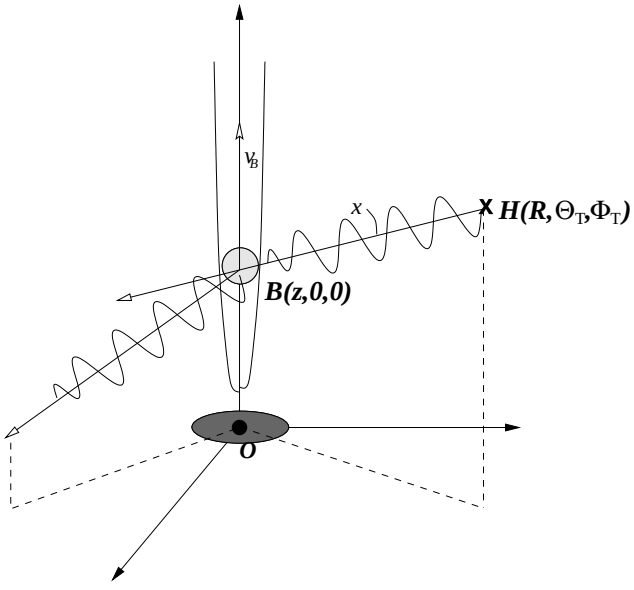

Fig. 1. Sketch of the basic geometry: The central black hole defines the origin *O* of the coordinate system. A photon, emitted at an arbitrary point *H* with the spherical polar coordinates *R*, $\Theta_{\rm T}$ and $\Phi_{\rm T}$, is scattered within the plasmoid, called blob, which is located at point *B* at the distance *z* above the black hole and moves along its angular momentum axis with velocity $v_{\rm B} = B_\Gamma c$

2 General considerations

Figure 1 shows a sketch of the situation considered. The amount of the energy gain of the scattered photons depends on the geometrical relations as well as on the blob properties.

In general all quantities in the electron rest frame are indicated by a prime and those in the frame of the galaxy by an asterisk; quantities in the blob rest frame are not indexed. For simplicity we will perform the calculus in the rest frame of the blob. Therefore all quantities have to be transformed into the blob frame which we do using relativistic invariants. In the same way the results can be transformed into the frame of the galaxy respectively, and using a particular cosmological

model, into the frame of the observer.
We will first calculate the scattering rate for an arbitrarily placed point source; then the solution for an extended source can be derived by integrating the solution for a point source over the source distribution.

3 The differential scattering rate

The differential scattering rate, which is the angle-dependent photon number spectrum of the scattered photons, is in the blob frame given by (Dermer et al., 1992)

$$\dot{n}_{\rm S}(\epsilon_{\rm S},\Omega_{\rm S}) = c\int\limits_0^\infty d\epsilon \oint d\Omega \int\limits_1^\infty d\gamma \oint d\Omega_{\rm e} \times \quad (1-\beta\cos\psi)\, n_{\rm ph}(\epsilon,\Omega)\, n_{\rm e}(\gamma,\Omega_{\rm e})\, \frac{d^2\sigma}{d\epsilon_{\rm S} d\Omega_{\rm S}}. \quad (1)$$

Here, $n_{\rm ph}$ and $n_{\rm e}$ denote the differential number density of the incoming photons and the blob electrons, respectively. Since the scattering process is charge-independent, we don't distinguish electrons and positrons. The differential cross section $d^2\sigma/(d\epsilon_{\rm S} d\Omega_{\rm S})$ can be written in the Thomson limit ($\epsilon' = \gamma\epsilon(1-\beta\cos\psi) \leq 1$) using the head-on approximation as (Reynolds, 1982), (Dermer & Schlickeiser, 1993)

$$\frac{d^2\sigma}{d\epsilon_{\rm S} d\Omega_{\rm S}} \simeq \sigma_{\rm T}\delta\Big[\epsilon_{\rm S} - \gamma^2\epsilon(1-\beta\cos\psi)\Big] \times \delta(\mu_{\rm S}-\mu_{\rm e})\,\delta(\phi_{\rm S}-\phi_{\rm e}). \quad (2)$$

In the frame of the galaxy, the thermal photon point source at *H* provides in the blob at *B* a photon number density

$$n^*_{\rm H}(\epsilon^*,\mu^*,\phi^*) = \frac{\dot{N}_{\rm H}(\epsilon^*)}{4\pi x^2 c}\,\delta(\mu^*-\mu^*_{\rm H})\,\delta(\phi^*-\phi^*_{\rm H}). \quad (3)$$

where x denotes the distance between the photon source at *H* and the blob at *B* (cf. Fig.1). $\dot{N}_{\rm H}$ is the photon number spectrum of the photon source and c the speed of light. Using the invariance n/ϵ^2 (Rybicki & Lightman, 1979) and $\phi_{\rm H} = \phi^*_{\rm H}$ this relation can be transformed into the rest frame of the blob.
Assuming an isotropic power law energy distribution with a low and an high energy cut-off for the electrons within the blob, $n_{\rm e}(\gamma,\Omega_{\rm e}) = n_{\rm e}(\gamma) = n_{\rm e}^{(0)}/(4\pi)\,\gamma^{-s},\ \gamma_1 \leq \gamma \leq \gamma_2$, and a grey body (GB), $\dot{N}_{\rm H}(\epsilon^*)\big|_{\rm GB} = \dot{N}_{\rm H}^{(0)}\epsilon^{*2}(2\,\zeta(3)\,\Theta^3\,(e^{\frac{\epsilon^*}{\Theta}}-1))^{-1}$, as well as a monochromatic (MC) photon source spectrum, $\dot{N}_{\rm H}(\epsilon^*)\big|_{\rm MC} = \dot{N}_{\rm H}^{(0)}\delta(\epsilon^*-\langle\epsilon^*\rangle)$, integration of (1) and the transformation into the galactic frame gives in the case of a grey body photon source

$$\dot{n}^*_{\rm S}(\epsilon^*_{\rm S},\Omega^*_{\rm S})\Big|_{\rm GB} = \frac{D\,\sigma_{\rm T}\,n_{\rm e}^{(0)}\,\dot{N}_{\rm H}^{(0)}}{64\,\pi^2 x^2\,\zeta(3)\,\Theta}\left(\frac{\epsilon^*_{\rm S}}{\eta\,\Theta}\right)^{-\frac{s+1}{2}} \times \int\limits_{\epsilon^*_{\rm S}/(\eta\Theta\gamma_2^2)}^{\epsilon^*_{\rm S}/(\eta\Theta\gamma_1^2)} dt\,\frac{t^{\frac{s+3}{2}}}{e^t-1} \quad (4)$$

where $D \equiv [\Gamma(1-B_\Gamma\mu^*_{\rm S})]^{-1}$ denotes the Doppler factor and in the case of a monochromatic photon source

$$\dot{n}^*_{\rm S}(\epsilon^*_{\rm S},\Omega^*_{\rm S})\Big|_{\rm MC} = \frac{D\sigma_{\rm T} n_{\rm e}^{(0)}\dot{N}_{\rm H}^{(0)}}{32\,\pi^2 x^2\langle\epsilon^*\rangle}\left(\frac{\epsilon^*_{\rm S}}{\eta\,\langle\epsilon^*\rangle}\right)^{-\frac{s+1}{2}}, \quad \eta\langle\epsilon^*\rangle{\gamma_1}^2 \leq \epsilon^*_{\rm S} \leq \eta\langle\epsilon^*\rangle{\gamma_2}^2 \quad (5)$$

with

$$\eta \overset{\beta\to1}{\simeq} D^2\Big[1-\mu^*_{\rm S}\mu^*_{\rm H} - \sqrt{(1-\mu^{*2}_{\rm S})(1-\mu^{*2}_{\rm H})}\cos(\phi^*_{\rm S}-\phi^*_{\rm H})\Big] \quad (6)$$

The restriction in energy is a consequence of the cut-offs in the energy distribution of the electrons. With equations (4,5) we can calculate the differential photon number spectrum for target photons of an extended source by integration over the source distribution. Afterwards, the differential luminosity, i. e. the luminosity per solid angle element, can be derived by an energy integration. Since the integral over the source distribution is much simpler, when the energy integration is performed first, we will first derive the differential luminosity for a point source and then for an extended target photon source. The calculation of the differential photon number spectrum is performed in chapter 5.

4 The differential luminosity $dL^*_{\rm S}/d\Omega^*_{\rm S}$

The differential luminosity of the scattered photons in the galactic frame can be derived from

$$\frac{dL^*_{\rm S}}{d\Omega^*_{\rm S}} = D\,V_{\rm B}\int_0^\infty d\epsilon^*_{\rm S}\;\epsilon^*_{\rm S}\,\dot{n}^*_{\rm S}, \quad (7)$$

with the volume of the blob, $V^*_{\rm B} = DV_{\rm B}$ (Begelman et al., 1984). Inserting (4) and (5) in (7), respectively, we get the same differential luminosity for the monochromatic photon source as well as for a grey body spectrum.

$$\frac{dL^*_{\rm S}}{d\Omega^*_{\rm S}} = \frac{3\,\zeta(4)D^2V_{\rm B}\,\sigma_{\rm T}\,n_0\dot{N}_{\rm H}^{(0)}\,\Theta}{16\,\zeta(3)\pi^2}m_{\rm e}c^2 \times \frac{\eta^2}{x^2}\begin{cases}\frac{{\gamma_2}^{3-s}-{\gamma_1}^{3-s}}{3-s} & ,\ s\neq3\\ \ln\left(\frac{\gamma_2}{\gamma_1}\right) & ,\ s=3\end{cases} \quad (8)$$

Thus, the assumption of a monochromatic photon source as an approximation of a photon source radiating with a thermal spectrum has no impact on the differential luminosity of the inverse Compton scattered photons.

The luminosity of an extended photon source can be derived by integration over its surface, provided the photon source is optically thick. We approximate the surface of the dust torus by a spherical shell with a radius $R_{\rm DT}$ and an angular extent of $\Theta_{\rm T} = \Theta_0$ to $\Theta_{\rm T} = 180^\circ - \Theta_0$ and perform the integral $R^2\int_{-\tau}^{\tau}d\mu^*_{\rm T}\int_0^{2\pi}d\phi^*_{\rm T}\,dL^*_{\rm S}/d\Omega^*_{\rm S}$, $\tau = \cos\Theta_0$. Inserting the former result and making use of the relations $x^2 =$

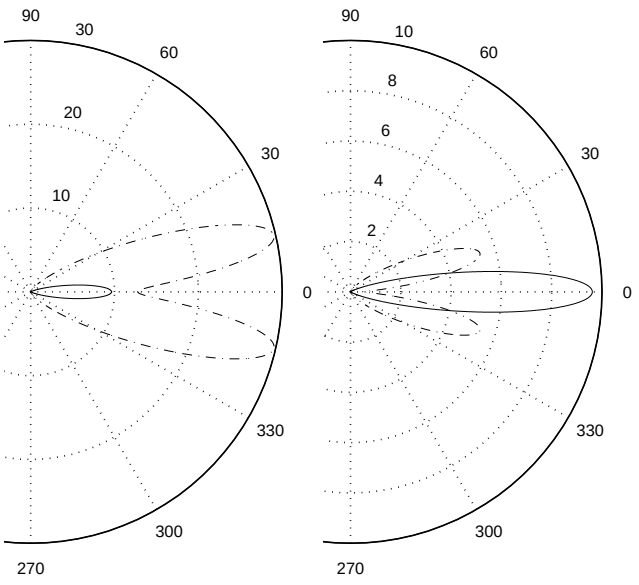

Fig. 2. The differential luminosity in arbitrary units as antenna diagrams for the dust torus (solid line) and the accretion disk (dash-dotted line) as target photon sources for different distances of the blob from the centre, F, measured in units of the accretion disk radius. The 0° direction defines the jet axis. Here we use an electron spectral index $s=3$ and for presentability $\Gamma=2.3$; for other parameters, see the text. *Left panel*: $F=4$; the scattered accretion disk emission dominates the differential luminosity. *Right panel*: $F=7$; the scattered dust emission is more intense than the accretion disk contribution for small angles and stays dominant also for greater distances. Note that the relative intensities of the two components scale with $L_{\rm DT}/L_{\rm AD}$.

$R_{\rm DT}^2 + z^2 - 2zR_{\rm DT}\mu_{\rm T}^*$, $\mu_{\rm H}^* = \frac{f-\mu_{\rm T}^*}{\sqrt{1+f^2-2\,f\,\mu_{\rm T}^*}}$ and $\phi_{\rm T}^* = \phi_{\rm H}^*$, where $f \equiv z/R_{\rm DT}$ is the height z of the blob normalised to $R_{\rm DT}$ we find

$$\left.\frac{dL_{\rm S}^*}{d\Omega_{\rm S}^*}\right|_{\rm DT} = \frac{\rho_3}{\rho_1}\,\frac{3\,V_{\rm B}\,\sigma_{\rm T}\,n_{\rm e}^{(0)}\,(\dot{N}_{\rm H}^{(0)}\,\Theta)_{\rm DT}\,\zeta(4) m_{\rm e}c^2}{16\,\zeta(3)\,\pi}\,D^6$$
$$\times\quad \frac{1}{f}\left[\frac{3\mu_{\rm S}^{*\,2}-1}{8f^2}\,(o-u)\left(1+\frac{(1-f^2)^2}{ou}\right)\right.$$
$$+\left((1+\mu_{\rm S}^{*\,2})-(1+f^2)\,\frac{3\mu_{\rm S}^{*\,2}-1}{4f^2}\right)\ln\left(\frac{o}{u}\right)$$
$$\left.-\,2\,\frac{\mu_{\rm S}^*}{f}\left(\sqrt{o}-\sqrt{u}\right)\left(1+\frac{1-f^2}{\sqrt{o\,u}}\right)\right] \qquad (9)$$

with

$$\rho_{\rm m} \equiv \begin{cases} \frac{{\gamma_2}^{m-s}-{\gamma_1}^{m-s}}{m-s} & ,\quad s\neq m \\ \ln\left(\frac{\gamma_2}{\gamma_1}\right) & ,\quad s=m \quad . \end{cases} \qquad (10)$$

and $o \equiv f^2+1+2f\tau$ and $u \equiv f^2+1-2f\tau$. For the accretion disk we calculate $\int_0^{R_{\rm AD}} dR \int_0^{2\pi} d\phi_{\rm T}^*\, R\, dL_{\rm S}^*/d\Omega_{\rm S}^*$ and obtain

$$\left.\frac{dL_{\rm S}^*}{d\Omega_{\rm S}^*}\right|_{\rm AD} = \frac{\rho_3}{\rho_1}\,\frac{3\,V_{\rm B}\,\sigma_{\rm T}\,n_{\rm e}^{(0)}\,(\dot{N}_{\rm H}^{(0)}\,\Theta)_{\rm AD}\,\zeta(4) m_{\rm e}c^2}{32\,\zeta(3)\,\pi}\,D^6$$
$$\times\quad \left[(3\mu_{\rm S}^{*\,2}-1)\,\frac{1}{F^2+1}+8\mu_{\rm S}^*\left(\frac{F}{\sqrt{F^2+1}}-1\right)\right.$$
$$\left.+\,(3-\mu_{\rm S}^{*2})\,\ln\left(\frac{F^2+1}{F^2}\right)\right],\ F\equiv\frac{z}{R_{\rm AD}} \qquad (11)$$

5 The differential photon number spectrum

Similar to the calculation of the differential luminosity, the differential photon number spectrum of an extended source can be derived by the integration $DV_{\rm B}\int dA\ \dot{n}_{\rm S}^*$. As seen in the calculation above, the two considered target photon spectra (GB and MC) gave the same differential luminosity. For the monochromatic case an analytic solution for the differential scattering rate can be derived, so we concentrate on this case.

Note that η (cf. (6)) in the energy interval of the differential scattering rate $\dot{n}_{\rm S}^*$ in (5) depends on both integration variables. So, we first average η over $\phi_{\rm T}^*$: $\langle\eta\rangle = D^2\left[1-\mu_{\rm S}^*\mu_{\rm H}^*\right]$. Because the system is symmetric to the jet axis this seems to be a good approximation.

The radiation of the counter-jet is highly suppressed because of the angular dependence of the Doppler factor D. For simplicity, we consider scattering angles smaller than $\Theta_{\rm S}=90^\circ$ and distances of the blob smaller than the distance to the torus $z \le R_{\rm DT}$. Other values of $\Theta_{\rm S}$ and z can easily be taken into account.

For the integral no analytical solution can be found for arbitrary values of s. To make progress, we assume that the spectral index of the electron distribution is $s=3$. Setting $\eta \equiv \langle\eta\rangle$ in (5) the two limits can be inside or outside the integration interval. Therefore the solution for the differential photon number spectrum after integration splits into three parts:

$$\left.\dot{N}_{\rm S}^*\right|_{\rm DT} = \frac{V_{\rm B}\,\sigma_{\rm T}\left(\dot{N}_{\rm H}^{(0)}\langle\epsilon^*\rangle\right)_{\rm DT}}{32\,\pi^2}\,\frac{n_{\rm e}^{(0)}}{\rho_1}\,D^6\,\epsilon_{\rm S}^{*\,-2}$$
$$\times\,\frac{1}{f}\left[\frac{\mu_{\rm S}^{*\,2}}{8\,f^2}\,(o^2-u^2)\left(1+\frac{(1-f^2)^2}{o^2u^2}\right)\right.$$
$$-\,\frac{\mu_{\rm S}^*}{2\,f}\,(o-u)\left(1+\frac{1-f^2}{o\,u}\right)$$
$$\left.+\,\left(1-\frac{\mu_{\rm S}^{*\,2}}{2\,f^2}\,(1-f^2)\right)\ln\left(\frac{o}{u}\right)\right]$$

$$\text{with} \quad \left\{ \begin{array}{l} o = T_+ \\ u = t^+_{\gamma_1} \end{array} \right\} \quad \text{for } {\gamma_1}^2\, A_+ \le \epsilon^*_{\rm S} \le {\gamma_1}^2\, A_- \qquad \left\{ \begin{array}{l} o = T_+ \\ u = T_- \end{array} \right\} \quad \text{for } {\gamma_1}^2\, A_- \le \epsilon^*_{\rm S} \le {\gamma_2}^2\, A_+ \qquad \left\{ \begin{array}{l} o = t^+_{\gamma_2} \\ u = T_- \end{array} \right\} \quad \text{for } {\gamma_2}^2\, A_+ \le \epsilon^*_{\rm S} \le {\gamma_2}^2\, A_- \,. \tag{12}$$

For clarity we defined the functions $A_\pm = A_\pm(f, \mu^*_{\rm S})$,

$$A_\pm \equiv D^2\, \langle \epsilon^* \rangle_{\rm DT} \left(1 - \mu^*_{\rm S}\, \frac{f \pm \tau}{\sqrt{1 + f^2 \pm 2\, f\, \tau}} \right), \tag{13}$$

which carry the information about the position of the blob and the aspect angle and

$$t^\pm_{\gamma_{1|2}} \equiv \frac{f}{\mu^*_{\rm S}} \left(1 - \frac{\epsilon^*_{\rm S}}{D^2\, \langle \epsilon^* \rangle_{\rm DT}\, {\gamma_{1|2}}^2} \right) \pm \sqrt{\frac{f^2}{{\mu^*_{\rm S}}^2} \left(1 - \frac{\epsilon^*_{\rm S}}{D^2 \langle \epsilon^* \rangle_{\rm DT} {\gamma_{1|2}}^2} \right)^2 + 1 - f^2}\,, \tag{14}$$

$$T_\pm \equiv \sqrt{1 + f^2 \pm 2\, f\, \tau}\,. \tag{15}$$

Similarly, we find for the accretion disk as target photon source

$$\left. \dot{N}^*_{\rm S} \right|_{\rm AD} = \frac{V_{\rm B}\, \sigma_{\rm T}\, n_{\rm e}^{(0)}\, \left(\dot{N}_{\rm H}^{(0)} \langle \epsilon^* \rangle \right)_{\rm AD}}{32\, \pi^2}\, D^6\, {\epsilon^*_{\rm S}}^{-2} \times \left[\ln\left(\frac{o}{u} \right) - 2\,(o - u) + \frac{1}{2}\,(o^2 - u^2) \right]$$

$$\text{with} \quad \left\{ \begin{array}{l} o = L_+ \\ u = l_{\gamma_1} \end{array} \right\} \quad \text{for } {\gamma_1}^2\, B_+ \le \epsilon^*_{\rm S} \le {\gamma_1}^2 B_- \qquad \left\{ \begin{array}{l} o = L_+ \\ u = L_- \end{array} \right\} \quad \text{for } {\gamma_1}^2 B_- \le \epsilon^*_{\rm S} \le {\gamma_2}^2 B_+ \qquad \left\{ \begin{array}{l} o = l_{\gamma_2} \\ u = L_- \end{array} \right\} \quad \text{for } {\gamma_2}^2 B_+ \le \epsilon^*_{\rm S} \le {\gamma_2}^2 B_- \,. \tag{16}$$

The function $B_\pm = B_\pm(F, \mu^*_{\rm S})$, $l_{1|2}$ and $L_\pm$ are defined as

$$B_\pm \equiv D^2\, \langle \epsilon^* \rangle_{\rm AD}\, (1 - L_\pm)\,, \tag{17}$$

$$l_{\gamma_{1|2}} \equiv 1 - \frac{\epsilon^*_{\rm S}}{D^2 \langle \epsilon^* \rangle_{\rm AD} {\gamma_{1|2}}^2}\,, \tag{18}$$

$$L_- \equiv \frac{\mu^*_{\rm S} F}{\sqrt{1 + F^2}} \quad \text{and} \quad L_+ \equiv \mu^*_{\rm S}\,. \tag{19}$$

For a more detailed discussion of the presented results see Arbeiter et al. (submitted to A&A).

6 Summary

We have calculated comptonization γ-ray spectra of AGNi for arbitrary observing angles. We present analytical solutions for the bolometric luminosity and the photon number spectrum produced by inverse-Compton scattering for an arbitrarily placed point source of target photons as well as for the accretion disk and a dust torus as the target photon source. Our study does not rely on a specific model for the injection or acceleration of relativistic electrons in the jets of AGN. Therefore our results can also be used to determine EIC spectra in blast wave models for AGN and GRB (Pohl & Schlickeiser, 2000).

In agreement with previous studies, our results show that the highest differential luminosity and photon energy is emitted along the jet axis and for small distances to the accretion disk. Moreover, we point out that the scattered dust emission is concentrated on small aspect angles, whereas the scattered accretion disk photons show a broader distribution in aspect angle. For small aspect angles the relative relevance of the dust torus and the accretion disk depends sensitively on the distance of the blob from the accretion disk. Thus for small angles to the jet axis and distances of more than a few accretion disk radii the dust surrounding the AGNi is more important as target photon source for the inverse-Compton scattering.

A strong external photon field is likely to be found in FSRQ/OVV, in contrast to the case of BL Lacs. It may be concluded that the FSRQ/OVV observed with EGRET, i.e. the brightest ones, are those seen nearly head-on, in which case we probably observe comptonized dust emission. The FSRQ/OVV seen at an intermediate angle $\Theta^* \approx 10^\circ$ would show a significant level of scattered accretion disk emission. The latter objects are less intense, meaning they would be less likely identified as point sources, but would contribute to the extragalactic γ-ray background (Sreekumar et al., 1998).

Acknowledgements. We gratefully acknowledge financial support by the Bundesministerium für Bildung und Forschung through DESY, grant Verbundforschung 05AG9PCA.

References

Arbeiter, C., Pohl, M., Schlickeiser, R., (submitted to A&A)
Begelman,M. C., Blandford, R. D., Rees, M. J., 1984, Rev. Mod. Phys, 56, 255
Dermer, C. D., Schlickeiser, R., Mastichiadis, A., 1992, A&A, 256, L27
Dermer, C. D., Schlickeiser, R., 1993, ApJ, 416, 458
Maraschi, L., Ghisellini, G., Celotti, A., 1992, ApJ, 397, L5
Pohl, M., Schlickeiser, R., 2000, A&A, 354, 395
Rybicki, G. B., Lightman, A. P., 1979, Radiative Processes in Astrophysics, New York: John Wiley & Sons
Reynolds, G. B., 1982, ApJ, 256, 38
Sreekumar P., Bertsch, D.L., Dingus, B.L., et al., 1998, ApJ, 494, 523